International Journal of Multiphase Flow 79 (2016) 23–30

Contents lists available at ScienceDirect

International Journal of Multiphase Flow

journal homepage: www.elsevier.com/locate/ijmultiphaseflow

Shapes of ellipsoidal bubbles in infinite stagnant liquids

S. Aoyama, K. Hayashi, S. Hosokawa, A. Tomiyama*

Graduate School of Engineering, Kobe University, 1-1, Rokkodai, Nada, Kobe 657-8501, Japan

ARTICLE INFO

Article history:
Received 3 June 2015
Revised 1 September 2015
Accepted 12 October 2015
Available online 30 October 2015

Keywords:
Bubble
Shape
Aspect ratio
Correlation

ABSTRACT

Aspect ratios E of ellipsoidal bubbles in infinite stagnant clean liquids are measured for $\log M = -6.6$, -5.5, -4.9 and -3.9, where M is the Morton number. An empirical correlation of E applicable to a wide range of the Morton number is proposed by making use of the present data and Sugihara's data at $\log M = -11$ (2007). The aspect ratio in this correlation is expressed in terms of the combination of the Eötvös number and the bubble Reynolds number to account for the effects of the inertial, viscous, buoyant and surface tension forces on E. Terminal velocities of ellipsoidal bubbles are accurately predicted by using the proposed correlation and a drag correlation proposed by Rastello et al. (2011).

Introduction

The shape of a bubble is one of the most important factors affecting bubble motion and heat and mass transfer from the bubble (Clift et al., 1978). The shape of a free rising bubble in an infinite stagnant liquid is known to depend on the bubble Reynolds number Re, the Eötvös number Eo and the Morton number M. Grace et al. (1976) proposed a graphical correlation of Re and the bubble shape in terms of Eo and M for $10^{-2} < Eo < 10^{3}$, $10^{-14} < M < 10^{8}$ and $10^{-1} < Re < 10^{5}$. Bubble shapes appearing in these ranges are spherical, ellipsoidal, wobbling, dimpled ellipsoidal-cap, skirted and spherical-cap.

The shape of an ellipsoidal bubble is characterized by the aspect ratio, E, which is the ratio of the maximum vertical dimension to the maximum horizontal dimension. Forces acting on a bubble such as the drag, lift and virtual mass forces have often been expressed in terms of E. Moore (1965) derived a drag coefficient C_D of an ellipsoidal bubble in the viscous force dominant regime in terms of Re and E. Tomiyama et al. (2002a) and Tomiyama (2004) also proposed a C_D model for bubbles in the surface tension dominant regime in terms of Eo and E. Tomiyama et al. (2002b) confirmed that the lift coefficient of a bubble is positive when the bubble is small and spherical, whereas it decreases to a negative value as E decreases with increasing the bubble diameter. It is well known that the virtual mass coefficient of a sphere is 1/2. The virtual mass coefficient of an ellipsoidal bubble is however given as a tensor, of which the components are functions of E (Lamb, 1932; Tomiyama, 2004). The aspect ratio also plays an important role in the heat and mass transfer, e.g. the mass transfer coefficient of an ellipsoidal bubble is expressed in terms of E, Re and the Schmidt number (Lochiel and Calderbank, 1964).

The knowledge on E is therefore of great importance in evaluating forces acting on a bubble and heat and mass transfer coefficients as well. Many studies on E have been carried out so far (Tadaki and Maeda, 1961; Moore, 1965; Wellek et al., 1966; Vakrushev and Efremov, 1970; Fan and Tsuchiya, 1990; Duineveld 1995; Kushch et al., 2002; Okawa et al., 2003; Myint et al., 2007; Sugihara et al., 2007; Legendre et al., 2012; Liu et al., 2015). Moore (1965) derived a model of E, which is a simple function of the bubble Weber number We, for bubbles of small deformation. Sugihara et al. (2007) measured bubble shapes in super-purified water and extended Moore's model so as to be applicable to bubbles of $0.5 < E < 1$. These two correlations were however proposed for bubbles in low viscosity systems and viscous effects were not taken into account. Legendre et al. (2012) carried out experiments on ellipsoidal bubbles rising through viscous liquids. They extended the Moore model by introducing a factor of M to account for the viscous effect on bubble shape. Liu et al. (2015) recently measured bubble aspect ratios for $10^{-4} < M < 10^{1}$ and $M = 10^{-11}$. They examined several combinations of relevant dimensionless groups for correlating E. The database of E in viscous liquids are however still insufficient, and the validity of the above correlations has not been examined sufficiently.

Shapes of single bubbles rising through infinite stagnant clean liquids were measured in this study for $10^{-7} < M < 10^{-3}$. The applicability of available correlations of E to the present data was examined. Then a correlation of E accounting for the viscous effect was proposed. The proposed correlation was applied to evaluate the bubble terminal velocity by combining the drag correlation proposed by Rastello et al. (2011).

* Corresponding author. Tel./fax: +81 78 803 6131.
E-mail address: tomiyama@mech.kobe-u.ac.jp (A. Tomiyama).

http://dx.doi.org/10.1016/j.ijmultiphaseflow.2015.10.003
0301-9322/

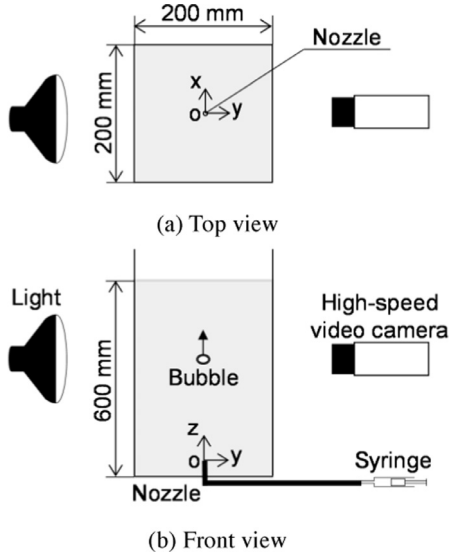

Fig. 1. Experimental setup (a) Top view, (b) Front view.

Table 1
Fluid properties at 25 °C.

log M	Glycerol concentration [wt.%]	ρ_L [kg/m^3]	μ_L [Pa s]	ρ_G [kg/m^3]	μ_G [Pa s]	σ [N/m]
−6.6	62	1155	0.0098	1.2	1.8×10^{-5}	0.0670
−5.5	70	1178	0.018	1.2	1.8×10^{-5}	0.0667
−4.9	75	1191	0.026	1.2	1.8×10^{-5}	0.0666
−3.9	80	1204	0.045	1.2	1.8×10^{-5}	0.0662

Experimental

Experimental setup

Fig. 1 shows the experimental setup. The width, depth and height of the tank made of transparent acrylic resin were 0.20, 0.20 and 0.63 m, respectively. The maximum bubble diameter in the present experiment was 6.11 mm. The tank size was therefore large enough to make the wall effect on the bubble motion and shape negligible (Clift et al., 1978).

Air and glycerol–water solutions were used for the gas and liquid phases, respectively. Water purified by a Millipore system (Elix 3) and clean glycerol (Kishida-Kagaku) were used for the glycerol–water solutions. The experiments were carried out at room temperature and atmospheric pressure. The liquid density and viscosity were measured using a densimeter (Ando Keiki Co., Ltd., JIS B7525) and a viscometer (A&D, SV-10), respectively. The surface tension was measured using capillary tubes. The liquid temperature was kept at 25 ± 0.5 °C. The liquid temperature was measured using a thermometer (Netsuken, SN3000) during the experiments. The uncertainties in the measured density, viscosity and surface tension estimated at 95% confidence were 0.01%, 1.3% and 2.3%, respectively.

Table 1 shows the fluid properties of glycerol-water solutions, where M is the Morton number defined by

$$M = \frac{\mu_L^4 \Delta\rho g}{\rho_L^2 \sigma^3} \tag{1}$$

where g is the acceleration of gravity, μ the viscosity, ρ the density, σ the surface tension, $\Delta\rho$ the density difference $\rho_L - \rho_G$, and the subscripts L and G denote the liquid and the gas phases, respectively.

Single bubbles were released from the nozzle tip by injecting air from the syringe. The inner diameter of the nozzle was varied from 0.51 to 2.84 mm to form single bubbles of various sizes, which resulted in $0.76 \leq d \leq 6.11$ mm, where d is the sphere-volume-equivalent bubble diameter. All bubbles in the experiments rose rectilinearly and their shapes were axisymmetric. Successive images of the bubbles were taken by using a high-speed video camera (Integrated Design Tools, M5; exposure time: 1/10,000 s, frame rate: 170 frames/s). The spatial resolution was varied from 0.63×10^{-2} to 1.07×10^{-2} mm/pixel, so that the number of pixels for d of the minimum bubble was 80.

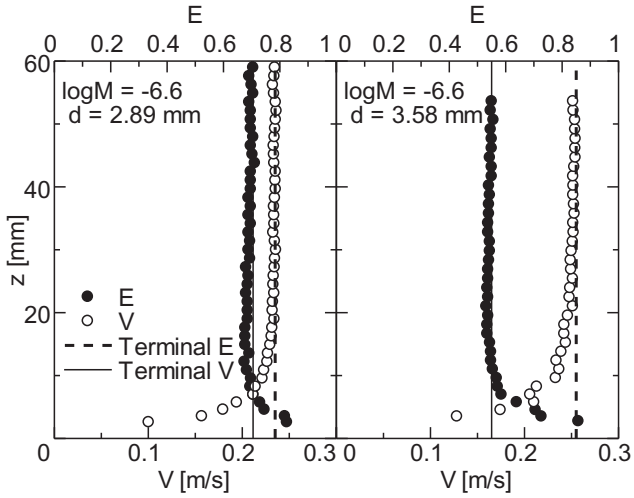

Fig. 2. Evolution of E and rising velocity V after bubble release.

The bubble diameters d, the bubble aspect ratios E and the bubble rising velocities V_T under terminal conditions were obtained by using an image processing method described in the following section. Examples of the measured aspect ratios and bubble rising velocities at $\log M = -6.6$ are shown in Fig. 2, where z is the vertical distance measured from the nozzle tip. In this lowest liquid viscosity system, the time constant of bubble rising motion was the largest in the fluid systems tested. The bubbles reached their terminal conditions at elevations less than 50 mm. Bubble images were therefore taken at 200 mm above the nozzle tip to assure that all the bubbles were in their terminal conditions. To check the axial symmetry of bubbles, an additional high-speed video camera was used to take their side images. Small differences between d and E calculated from the front and side images, i.e. less than 0.60% and 1.1% for d and E, confirmed that the bubbles were axisymmetric. The uncertainties in d, E and V_T estimated at 95% confidence were 1.5%, 2.5% and 0.89%, respectively.

Image processing

Detection of bubble interface

Images in the absence of bubbles were taken as background images before each measurement. The background subtraction was applied to each bubble image to clearly detect the bubble interface as shown in Fig. 3(a) and (b). The images after subtraction were transformed into binary images (Fig. 3(c)). The threshold of binarization was determined with the discriminant analysis method (Otsu, 1980). The interface was then detected by using a border following method and the pixels inside the bubble were filled up with a single color (Fig. 3(d)).

Calculation of geometric center of bubble image

The coordinates, $\boldsymbol{G}$ (= ($g_x(t)$, $g_z(t)$)), of the geometric center of the bubble image were calculated by

$$\boldsymbol{G} = \frac{\sum_{i=1}^{m}\sum_{k=1}^{m} \boldsymbol{r}_{i,k}\phi_{i,k}}{\sum_{i=1}^{m}\sum_{k=1}^{m} \phi_{i,k}} \tag{2}$$

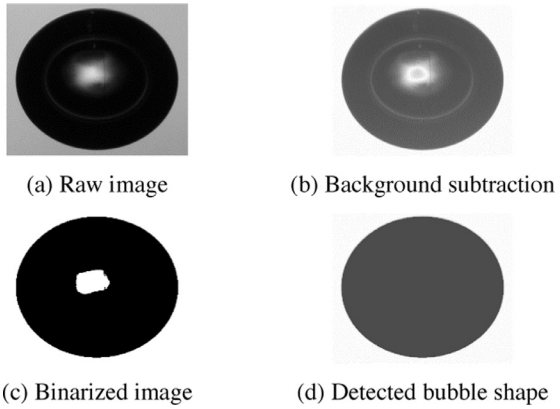

Fig. 3. Background subtraction and binarization (a) Raw image, (b) Background subtraction, (c) Binarized image, (d) Detected bubble shape.

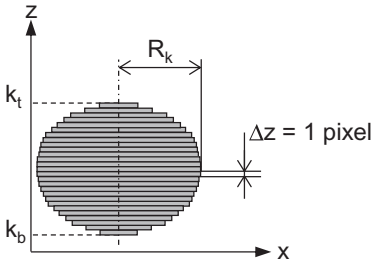

Fig. 4. Reconstruction of bubble shape.

where t is the time, ϕ the phase indicator ($\phi = 1$ for the gas phase and $\phi = 0$ for the liquid phase), $\boldsymbol{r}$ the position vector, the subscripts x and z are the horizontal and vertical coordinates, respectively, and the subscripts i and k are the pixel numbers in the x and z directions, respectively.

The instantaneous bubble rising velocity, $V(t)$, was calculated by $V(t) = [g_z(t) - g_z(t-\Delta t)]/\Delta t$, where Δt is the time interval between two successive images. The terminal velocity was then obtained by averaging $V(t)$.

Bubble diameter

Since bubble shapes were axisymmetric, they were reconstructed by piling up circular disks in the vertical direction from the bottom pixel k_b to the top pixel k_t as shown in Fig. 4. The thickness and radius of a disk were Δz (= 1 pixel) and R_k, respectively. The volume, Θ, of the reconstructed shape was given by

$$\Theta = \sum_{k=k_b}^{k_t} \pi {R_k}^2 \Delta z \tag{3}$$

Then d was calculated by using

$$d = \sqrt[3]{\frac{6\Theta}{\pi}} \tag{4}$$

It should be noted that d calculated using the above method agreed with those predetermined by a syringe as shown in Appendix A.1.

Aspect ratio

The maximum horizontal dimension, a, and the maximum vertical dimension, b, were measured by fitting a rectangle to the bubble as shown in Fig. 5. The bubble aspect ratio is defined by

$$E = \frac{b}{a} \tag{5}$$

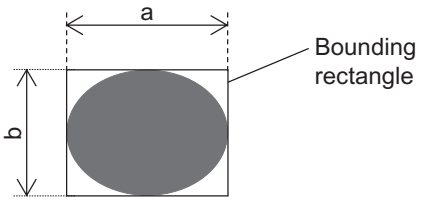

Fig. 5. Evaluation of bubble aspect ratio.

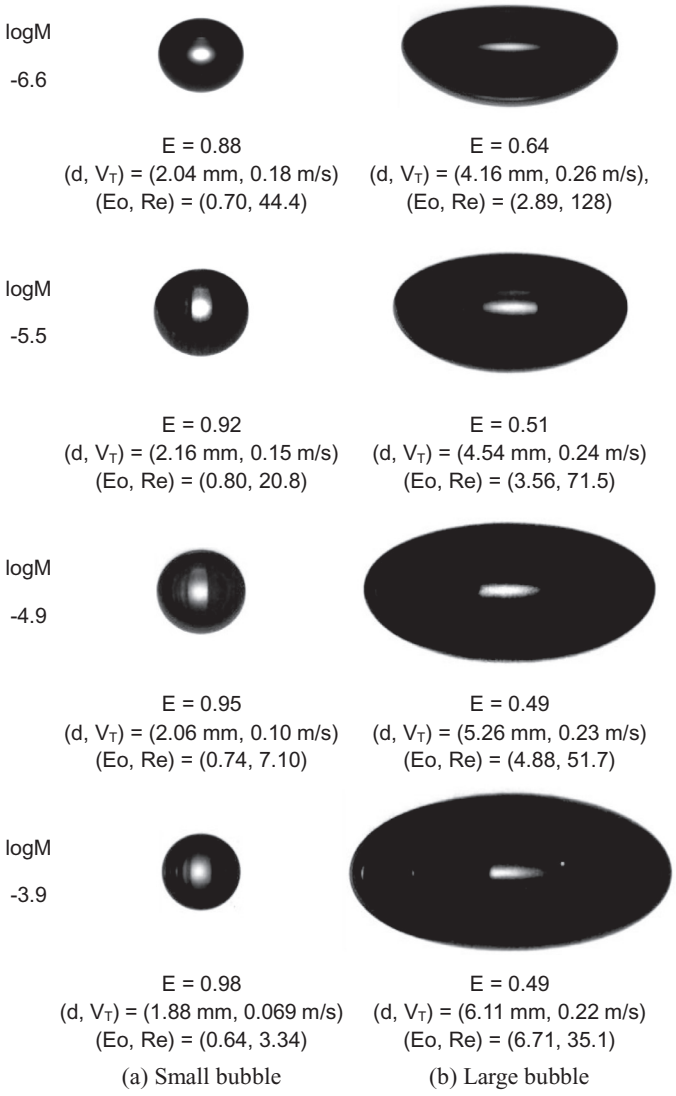

Fig. 6. Bubble images.

Results and discussion

Bubble aspect ratio and terminal velocity

Examples of the shapes of small and large bubbles are shown in Fig. 6, where *Eo* and *Re* are the Eötvös and Reynolds numbers defined by

$$Eo = \frac{\Delta\rho g d^2}{\sigma} \tag{6}$$

$$Re = \frac{\rho_L V_T d}{\mu_L} \tag{7}$$

The small bubble at the highest M is almost spherical ($E \approx 1$), whereas the decrease in M causes slight deformation. The larger bubbles are

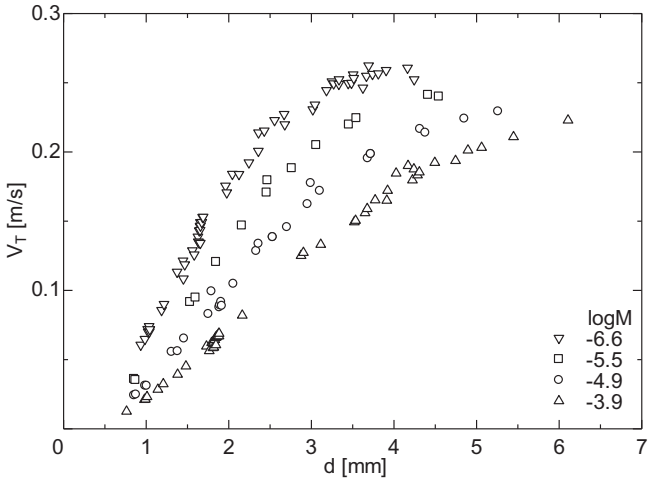

(a) Bubble terminal velocities

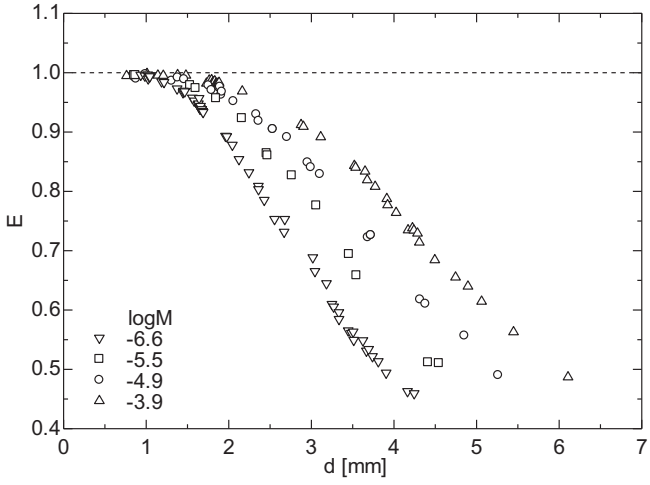

(b) Bubble aspect ratios

Fig. 7. Measured E and V_T (a) Bubble terminal velocities, (b) Bubble aspect ratios.

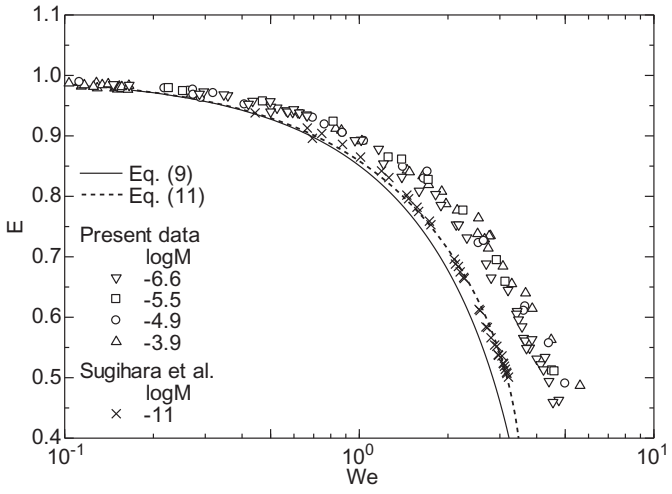

Fig. 8. Relation between E and We.

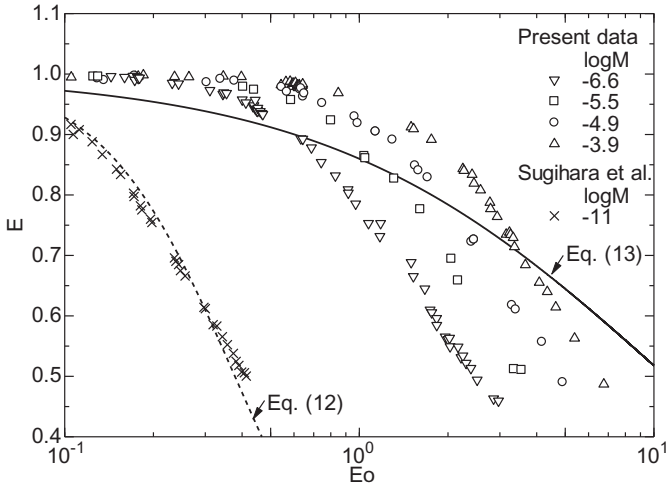

Fig. 9. Relation between E and Eo.

more flattened, and shape deformation becomes larger as M decreases.

Terminal velocities are shown in Fig. 7(a). The V_T increases with increasing d. The decrease in M increases V_T because of the decrease in the viscous force. As shown in Fig. 7(b), the bubble deformation becomes larger with increasing d, in other words with increasing V_T. This is because the dynamic pressure acting on the bubble nose (Moore, 1965) increases with V_T. As M increases, the shape deformation is mitigated due to the increase in the viscous force. All the data of E and V_T are given in Appendix A.2.

Comparisons with available correlations

The aspect ratios of bubbles have often been correlated in terms of the Weber number, which is defined as the ratio of the inertial force to the surface tension force:

$$We = \frac{F_i}{F_\sigma} = \frac{\rho_L V_T^2 d}{\sigma} \tag{8}$$

where F_i $(=\rho_L V_T^2 d^2)$ is the inertial force, and F_σ $(=\sigma d)$ the surface tension force. The measured E are plotted against We in Fig. 8. The aspect ratios at $\log M = -11$ measured by Sugihara et al. (2007) are also shown in the figure. Bubbles in this small M system are more flattened than those of the present data.

Moore (1965) derived the following relation between We and E from the balances between the dynamic pressure and the capillary pressure at the bubble nose and at the bubble side edge, respectively:

$$We = \frac{4E^{4/3}(E^{-3}+E^{-1}-2)}{(E^{-2}-1)^3}[E^{-2}\sec^{-1}E^{-1} - (E^{-2}-1)^{1/2}]^2 \tag{9}$$

which is applicable to bubbles of $\log M < -8$. He also derived the following solution for bubbles with very small shape deformation, i.e. for $We << 1$:

$$E = \left[1 + \frac{9}{64}We\right]^{-1} \tag{10}$$

Sugihara et al. (2007) introduced an additional term to the above solution to make it applicable to large Weber numbers as follows:

$$E = \left[1 + \frac{9}{64}We + \frac{0.04We^2}{(3.7-We)^{0.5}}\right]^{-1} \tag{11}$$

Eqs. (9) and (11) are compared with the data in the figure. Moore's model agree with Sugihara's data of low M at low We, whereas the difference between them becomes larger as We increases. Sugihara's data are, of course, well expressed with Eq. (11). However Eqs. (9) and (11) are not applicable to the present data because the viscous effect is neglected in Eqs. (9) and (11).

Sugihara et al. (2007) showed that their data could also be expressed in terms of the Eötvös number as shown in Fig. 9, where the

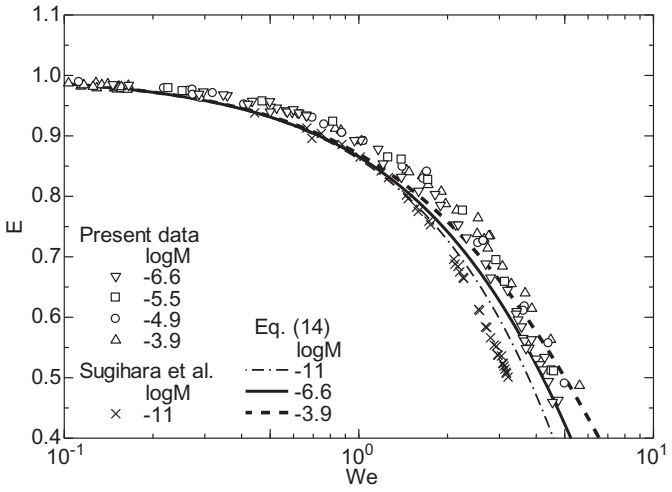

Fig. 10. Relation between E and We.

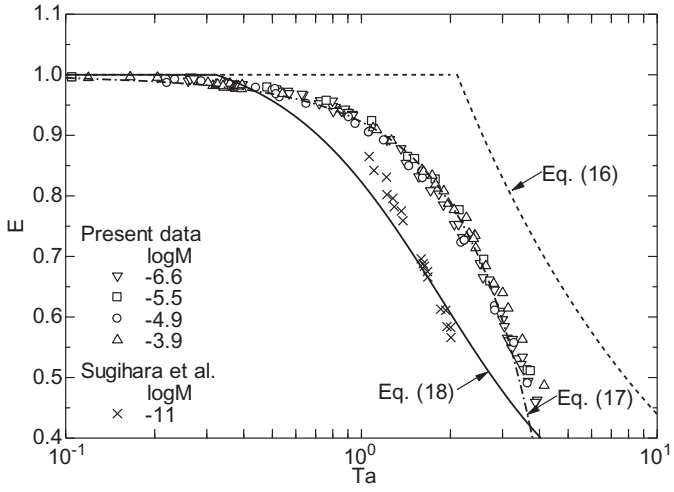

Fig. 11. Relation between E and Ta.

broken line is their correlation given by

$$E = \frac{1}{1 + 6.5Eo^{1.925}} \tag{12}$$

The Eötvös number is the ratio of the buoyant force F_b ($= \Delta\rho g d^3$) to the surface tension force: $Eo = F_b/F_\sigma = \Delta\rho g d^2/\sigma$. Wellek (1966) also expressed E in terms of Eo as follows:

$$E = \frac{1}{1 + 0.163Eo^{0.757}} \tag{13}$$

Although Eqs. (12) and (13) qualitatively agree with the data, the aspect ratios cannot be expressed only with Eo as shown in Fig. 9.

Legendre et al. (2012) extended the Moore's model, Eq. (10), so as to be applicable to bubbles in viscous liquids by introducing the Morton number into the correlation as follows:

$$E = 1 - \frac{9}{64}\left[\frac{We}{1 + 0.2M^{0.1}We}\right] \tag{14}$$

Since $We = F_i/F_\sigma$ and $M = {F_\mu}^4 F_b/{F_i}^2 {F_\sigma}^3$ where F_μ ($= \mu_L V_T d$) is the viscous force, the above correlation accounts for the effects of all the four forces acting on a bubble. This correlation is compared with the present data in Fig. 10. Although it gives a correct tendency for the viscous effect, i.e., E decreases with decreasing M, the aspect ratios are underestimated for $\log M = -3.9$ and -6.6, and overestimated for $\log M = -11$.

The Tadaki number Ta consists of the four relevant forces (Tadaki and Maeda, 1961):

$$Ta = ReM^{0.23} \tag{15}$$

where $Re = F_i/F_\mu = \rho_L V_T d/\mu_L$. This dimensionless group has been used in several correlations of E (Tadaki and Maeda, 1961; Vakrushev and Efremov, 1970; Fan and Tsuchiya 1990; Myint et al., 2007). Tadaki and Maeda (1961) proposed the following correlation of E for bubbles in various Morton number systems:

$$E^{1/3} = \begin{cases} 0.62 & \text{for } 16.5 < Ta \\ 1.36Ta^{-0.28} & \text{for } 6 < Ta \le 16.5 \\ 1.14Ta^{-0.176} & \text{for } 2 < Ta \le 6 \\ 1 & \text{for } Ta \le 2 \end{cases} \tag{16}$$

Myint et al. (2007) measured the aspect ratios of drops in infinite stagnant liquids. They pointed out that Ta is more appropriate to correlate E than We and Eo, and proposed the following correlation:

$$E = 1 - 0.0487Ta - 0.0289Ta^2 \tag{17}$$

Fan and Tsuchiya (1990) modified the E correlation for contaminated bubbles proposed by Vakrushev and Efremov (1970) to make it applicable to clean bubbles:

$$E = \begin{cases} 1 & \text{for } Ta \le 1 \\ [0.81 + 0.206\tanh\{2(0.8 - \log_{10}Ta)\}]^3 & \text{for } 1 \le Ta \le 39.8 \\ 0.24 & \text{for } Ta \ge 39.8 \end{cases} \tag{18}$$

The measured aspect ratios are plotted against Ta in Fig. 11. Although the present data for $-6.6 \le \log M \le -3.9$ are correlated in terms of Ta, the data of $\log M = -11$ largely differ from them. Hence the above correlations using only Ta cannot accurately evaluate E for a wide range of M.

Aspect ratio correlation applicable to bubbles in various liquid systems

The comparisons between the measured data and the available correlations in the previous section made it clear that the available correlations do not give good evaluations of E for a wide range of M. Since Eo and We do not include the viscous force, the correlations expressed in terms of Eo and/or We cannot account for the dependency of E on M. As mentioned above the Tadaki number consists of all the four forces acting on a bubble. However the aspect ratio data plotted against Ta still depend on M as shown in Fig. 11. This might be because Ta is weakly dependent on the viscous force. The Tadaki number can be expressed as

$$Ta = \frac{F_b^{0.23} F_i^{0.54}}{F_\sigma^{0.69} F_\mu^{0.08}} \tag{19}$$

which shows that the contribution of F_μ is much smaller than those of the other forces.

Even though Ta cannot correlate E in various M systems, the combinations of F_b and F_i in the numerator and of F_σ and F_μ in the denominator would be reasonable for correlating E because the increases in F_b and F_i decrease E whereas those in F_σ and F_μ increase E. Let us therefore consider a dimensionless group defined by

$$\Omega = \frac{{F_b}^\alpha {F_i}^\beta}{{F_\sigma}^\gamma {F_\mu}^\delta} \quad (\alpha, \beta, \gamma, \delta > 0) \tag{20}$$

where, in order to keep Ω dimensionless, the coefficients α, β, γ and δ should satisfy

$$\alpha + \beta = \gamma + \delta \tag{21}$$

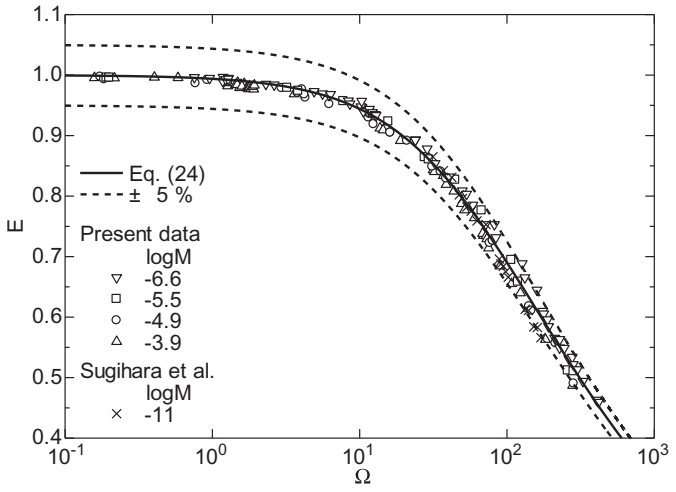

Fig. 12. Comparison between Eq. (24) and experimental data.

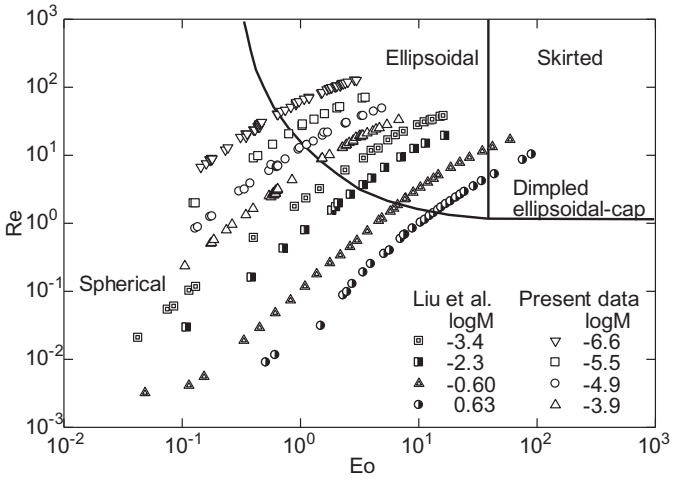

Fig. 13. Shape regime map.

Then, by referring to available correlations, let us assume the following functional form of E:

$$E = \frac{1}{[1 + p\Omega]^q} \tag{22}$$

where p and q should be positive since E decreases as Ω increases. The coefficients, α, β, γ, δ, p and q, were determined by applying the least-square fitting to all the experimental data. The resulting values are $(\alpha, \beta, \gamma, \delta, p, q) = (1.12, 1.00, 1.12, 1.00, 0.016, 0.388)$. Thus Ω is given by

$$\Omega = \frac{F_b^{1.12} F_i^{1.00}}{F_\sigma^{1.12} F_\mu^{1.00}} = Eo^{1.12} Re \tag{23}$$

and E is given by

$$E = \frac{1}{[1 + 0.016 Eo^{1.12} Re]^{0.388}} \tag{24}$$

All the measured aspect ratios are plotted against Ω in Fig. 12. The data are collapsed into a single curve. Eq. (24) gives good evaluations of E, the errors of which are to within ±5%.

Applicability of Eq. (24) to higher M systems

Liu et al. (2015) measured E of bubbles at M higher ($\log M = -3.4$, -2.3, -0.60 and 0.63) than those in the present experiments. Fig. 13 shows the present and Liu's data on the so-called Grace map. Our data are in the spherical bubble and the ellipsoidal bubble regimes. The data of Liu et al. are also in these regimes except for several data, which are in between the dimpled ellipsoidal-cap and skirted bubble regimes. The latter data are omitted in the following comparisons. Though the proposed correlation was based on the data of $\log M \leq -3.9$, the agreement with Liu's data is also good as shown in Fig. 14. The comparisons in Figs. 12 and 14 have confirmed that the dimensionless group $\Omega = Eo^{1.12} Re$ is of great use for correlating E for a wide range of the dimensionless groups, i.e. $-11 \leq \log M \leq 0.63$, $3.2 \times 10^{-3} \leq Re \leq 1.3 \times 10^2$ and $4.2 \times 10^{-2} \leq Eo \leq 2.9 \times 10^1$.

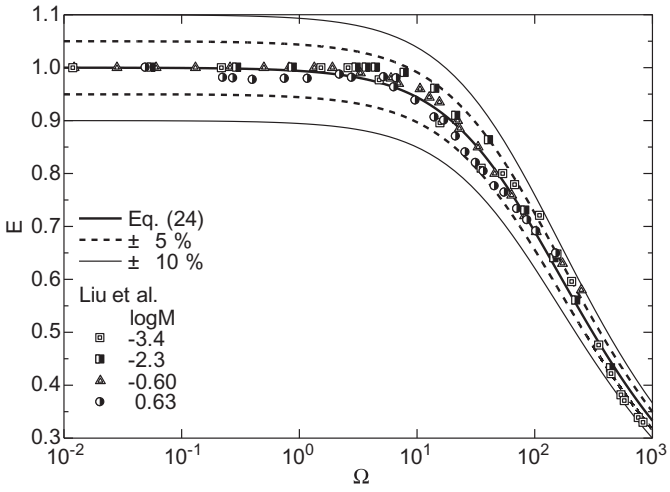

Fig. 14. Comparison between Eq. (24) and Liu's data.

Evaluation of V_T using proposed correlation of E

Application of the proposed correlation of E to the evaluation of the terminal velocity is carried out in the following. Rastello et al. (2011) proposed the following C_D correlation for clean ellipsoidal bubbles expressed in terms of Re and E:

$$C_D = \frac{16}{Re}\left[\frac{1 + 8/15(E^{-1} - 1) + 0.015(3G(E) - 2)Re}{1 + 0.015Re} + \left[\frac{8}{Re} + \frac{1}{2}\left(1 + \frac{3.315H(E)G(E)}{Re^{1/2}}\right)\right]^{-1}\right] \tag{25}$$

where $G(E)$ and $H(E)$ are given by (Moore, 1965; Sugihara et al., 2007)

$$G(E) = \frac{E^{-4/3}(E^{-2} - 1)^{3/2}[(E^{-2} - 1)^{1/2} - (2 - E^{-2})arc\sec E^{-1}]}{3[E^{-2} arc\sec E^{-1} - (E^{-2} - 1)^{1/2}]^2} \tag{26}$$

$$H(E) = 0.0108E^{-4} - 0.157E^{-3} + 1.5725E^{-2} - 2.0195E^{-1} - 1.617 \tag{27}$$

Terminal velocities calculated by using Eqs. (24) and (25) are compared with the data in Fig. 15, in which V_T calculated using other E correlations are also shown. The combination of Rastello's C_D model and the proposed correlation of E gives good evaluations of V_T.

The proposed correlation of E would be useful to evaluate other forces, i.e. the lift and virtual mass forces, and the heat and mass transfer coefficients of ellipsoidal bubbles by combining Eq. (24) with correlations for these forces and coefficients accounting for the effects of E.

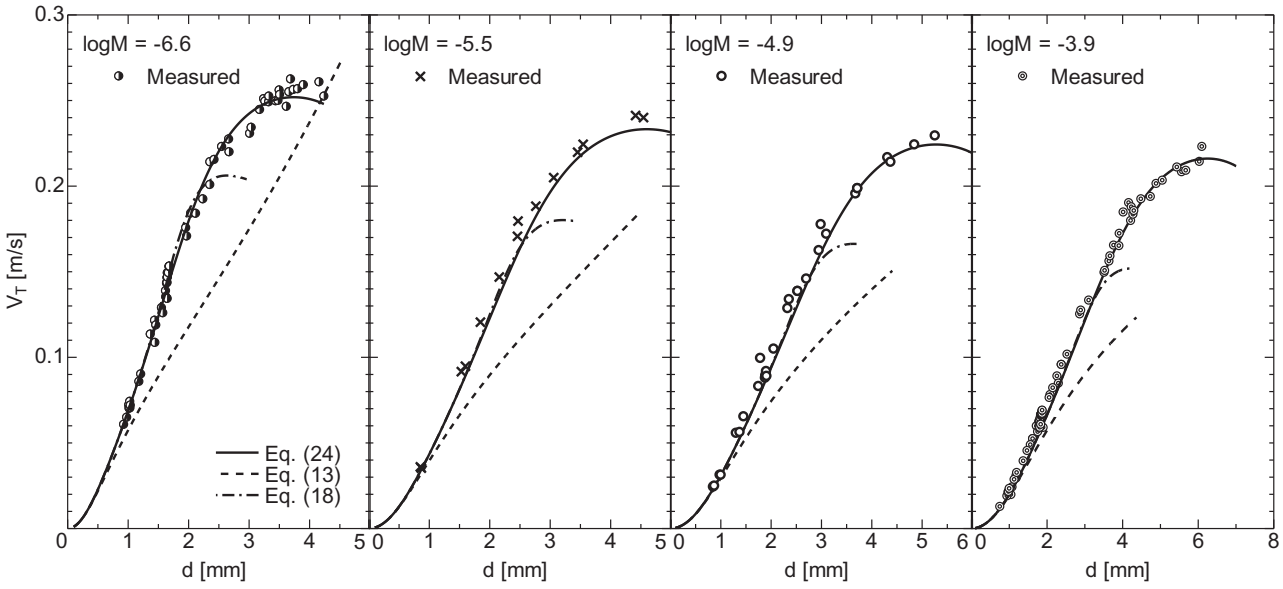

Fig. 15. Terminal velocities calculated by using Eq. (25) and various correlations of E.

Conclusions

Shapes of single bubbles rising through infinite stagnant clean liquids were measured by using a high-speed video camera for a wide range of fluid properties to investigate effects of the fluid properties on the bubble aspect ratio, E. The aspect ratios were evaluated from the bubble images by using an image processing method. The validity of available correlations were examined through comparisons with the data. The following dimensionless group was then introduced to correlate the bubble aspect ratios in various fluid property systems: $\Omega = Eo^{1.12}Re$, where Eo is the Eötvös number and Re is the bubble Reynolds number. As a result, the following conclusions were obtained:

(1) Though the Tadaki number Ta accounts for effects of all the relevant forces, i.e. the inertial, viscous, buoyant and surface tension forces, the aspect ratios in various Morton number systems were not well correlated only with Ta. This must be because the contribution of the viscous force in Ta is too small for correlating E of various viscosity systems.
(2) The proposed dimensionless group Ω is of great use in correlating E of various Morton number systems.
(3) The following correlation of E was proposed:

$$E = \frac{1}{[1 + 0.016Eo^{1.12}Re]^{0.388}}$$

The applicable range of this correlation is $-11 \le \log M \le 0.63$, $3.2 \times 10^{-3} \le Re \le 1.3 \times 10^{2}$ and $4.2 \times 10^{-2} \le Eo \le 2.9 \times 10^{1}$.
(4) The combination of the proposed correlation of E and a drag correlation proposed by Rastello et al. (2011) can give good evaluations of the terminal velocities of ellipsoidal bubbles.

Acknowledgments

The authors would like to express their thanks to Mr. Toshihiko Takegawa for his assistance. This work was supported by JSPS KAKENHI Grant number 15H03920.

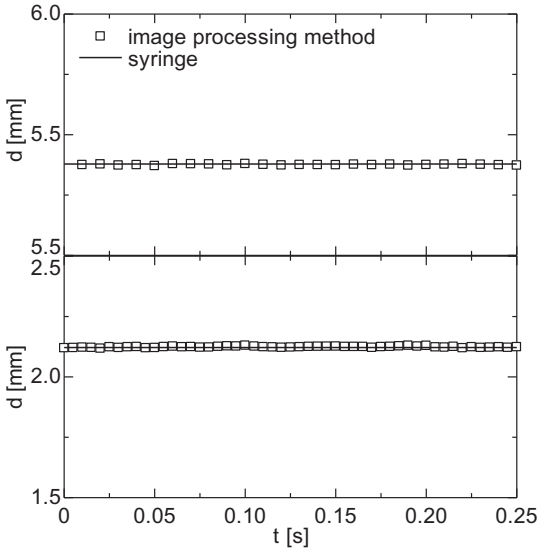

Fig. A1. Comparisons between bubble diameters calculated using the image processing method and the syringe.

Appendix

A.1 Validation of the image processing method

Validation of the image processing method for diameter measurement was carried out as follows. Predetermined amount of air was stored in a micro syringe (Hamilton, gastight 1705RN, Volume: 0.050 ml). The stored gas was then put into the test section filled with the stagnant liquid as a single bubble, d of which was also measured using the image processing method and was compared with that measured using the syringe. Fig. A.1 shows examples of the comparisons for $d = 5.38$ and 2.12 mm, where t is the time. The diameters obtained using the image processing method agree very well with those using the syringe, i.e. the errors were less than 0.5%. Hence the image processing method can accurately evaluate d.

Table A1
Bubble aspect ratio.

d [mm]	V_T [m/s]	E	d [mm]	V_T [m/s]	E	d [mm]	V_T [m/s]	E	d [mm]	V_T [m/s]	E	d [mm]	V_T [m/s]	E
	$\log M = -6.6$		2.12	0.184	0.854	1.60	0.095	0.974	2.99	0.178	0.841	1.87	0.067	0.978
0.934	0.061	0.996	2.24	0.192	0.832	1.85	0.121	0.957	3.10	0.172	0.829	1.88	0.069	0.977
0.985	0.065	0.995	2.36	0.201	0.809	2.16	0.147	0.924	3.68	0.195	0.723	1.88	0.067	0.981
1.02	0.072	0.996	2.36	0.214	0.803	2.46	0.171	0.864	3.72	0.199	0.726	1.88	0.069	0.983
1.02	0.070	0.990	2.43	0.215	0.785	2.47	0.180	0.861	4.32	0.217	0.618	2.16	0.082	0.969
1.04	0.074	0.995	2.55	0.223	0.753	2.76	0.188	0.827	4.38	0.214	0.611	2.88	0.125	0.912
1.04	0.070	0.993	2.67	0.227	0.732	3.06	0.205	0.776	4.85	0.224	0.557	2.90	0.127	0.909
1.04	0.072	0.994	2.68	0.220	0.753	3.45	0.220	0.694	5.26	0.229	0.490	3.11	0.133	0.892
1.19	0.086	0.985	3.02	0.231	0.688	3.54	0.224	0.659		$\log M = -3.9$		3.52	0.149	0.843
1.22	0.090	0.984	3.04	0.234	0.665	4.41	0.241	0.512	0.762	0.013	0.995	3.53	0.150	0.840
1.37	0.113	0.973	3.18	0.245	0.645	4.54	0.240	0.511	0.979	0.021	0.996	3.65	0.156	0.834
1.45	0.121	0.967	3.25	0.251	0.610		$\log M = -4.9$		0.990	0.021	0.996	3.68	0.159	0.819
1.45	0.108	0.969	3.27	0.249	0.605	0.853	0.024	0.993	1.01	0.023	0.998	3.77	0.165	0.808
1.47	0.119	0.968	3.33	0.249	0.596	0.876	0.025	0.990	1.14	0.028	0.996	3.91	0.165	0.788
1.56	0.129	0.958	3.33	0.252	0.584	0.987	0.031	0.997	1.21	0.032	0.995	3.92	0.172	0.777
1.58	0.126	0.953	3.45	0.250	0.565	1.01	0.031	0.993	1.38	0.039	0.996	4.03	0.185	0.764
1.63	0.139	0.946	3.49	0.250	0.561	1.31	0.056	0.987	1.48	0.045	0.996	4.17	0.190	0.735
1.63	0.135	0.948	3.51	0.256	0.563	1.38	0.056	0.992	1.73	0.060	0.982	4.22	0.180	0.738
1.64	0.134	0.957	3.51	0.253	0.549	1.46	0.065	0.989	1.76	0.056	0.987	4.24	0.188	0.734
1.64	0.143	0.942	3.62	0.246	0.549	1.75	0.083	0.979	1.79	0.062	0.988	4.28	0.183	0.729
1.65	0.146	0.939	3.67	0.255	0.531	1.79	0.099	0.971	1.81	0.058	0.984	4.31	0.185	0.714
1.65	0.143	0.940	3.69	0.262	0.534	1.89	0.088	0.975	1.81	0.062	0.979	4.49	0.192	0.684
1.65	0.134	0.940	3.74	0.256	0.522	1.89	0.089	0.976	1.81	0.063	0.984	4.75	0.194	0.655
1.66	0.149	0.939	3.81	0.257	0.513	1.91	0.092	0.963	1.82	0.059	0.984	4.90	0.201	0.640
1.66	0.147	0.944	3.90	0.259	0.494	1.92	0.089	0.968	1.83	0.064	0.986	5.06	0.203	0.614
1.67	0.149	0.938	4.16	0.261	0.463	2.06	0.105	0.952	1.84	0.066	0.979	5.45	0.211	0.563
1.68	0.153	0.935	4.24	0.252	0.459	2.33	0.128	0.930	1.84	0.061	0.982	6.11	0.223	0.487
1.69	0.153	0.933		$\log M = -5.5$		2.36	0.134	0.919	1.85	0.066	0.980			
1.96	0.175	0.893	0.853	0.036	0.996	2.53	0.139	0.905	1.85	0.066	0.977			
1.98	0.171	0.892	0.869	0.035	0.996	2.70	0.146	0.892	1.86	0.067	0.982			
2.04	0.184	0.878	1.53	0.092	0.979	2.95	0.162	0.849	1.86	0.067	0.980			

A.2 Experimental data of aspect ratios

All the data of terminal velocity and aspect ratio are given in Table A.1. These data would be of use not only for developing aspect ratio database for various fluid properties but also for validating numerical methods, e.g. interface tracking methods.

References

Clift, R., Grace, J.R., Weber, M.E., 1978. Bubbles, Drops, and Particles. Academic Press.

Duineveld, P.C., 1995. The rise velocity and shape of bubbles in pure water at high Reynolds number. J. Fluid Mech. 292, 325–332.

Fan, L.S., Tsuchiya, K., 1990. Bubble Wake Dynamics in Liquids and Liquid–Solid Suspensions. Butterworth-Heinemann.

Grace, J.R., Wairegi, T., Nguyen, T.H., 1976. Shapes and velocities of single drops and bubbles moving freely through immiscible liquids. Trans. Inst. Chem. Eng. 54, 167–173.

Kushch, V.I., Sangani, A.S., Spelt, P.D.M., Koch, D.L., 2002. Finite-Weber-number motion of bubbles through a nearly inviscid liquid. J. Fluid Mech. 460, 241–280.

Lamb, H., 1932. Hydrodynamics, 6th Edition Cambridge Univ. Press.

Legendre, D., Zenit, R., Velez-Cordero, J.R., 2012. On the deformation of gas bubbles in liquids. Phys. Fluids 24 ISSN 1070–6631.

Liu, L., Yan, H., Zhao, G., 2015. Experimental studies on the shape and motion of air bubbles in viscous liquids. Exp. Thermal Fluid Sci. 62, 109–121.

Lochiel, A.C., Calderbank, P.H., 1964. Mass transfer in the continuous phase around axisymmetric bodies of revolution. Chem. Eng. Sci. 19, 471–484.

Moore, D.W., 1965. The velocity of rise of distorted gas bubbles in a liquid of small viscosity. J. Fluid Mech. 23, 749–766.

Myint, W., Hosokawa, S., Tomiyama, A., 2007. Shape of single drops rising through stagnant liquids. J. Fluid Sci. Technol. 2, 184–195.

Okawa, T., Tanaka, T., Kataoka, I., Mori, M., 2003. Temperature effect on single bubble rise characteristics in stagnant distilled water. Int. J. Heat Mass Transfer 46, 903–913.

Otsu, H., 1980. An automatic threshold selection method based on discriminant and least squares criteria. Trans. Electro. Common. Eng. Jpn. D J63-D, 349–356 in Japanese.

Rastello, M., Marie, J., Lance, M., 2011. Drag and lift forces on clean spherical and ellipsoidal bubbles in a solid-body rotating flow. J. Fluid Mech. 682, 434–459.

Sugihara, K., Sanada, T., Shirota, M., Watanabe, M., 2007. Behavior of single rising bubbles in superpurified water. Soc. Chem. Eng. Jpn. 33, 402–408 in Japanese.

Tadaki, T., Maeda, S., 1961. On the shape and velocity of single air bubbles rising in various liquids. Soc. Chem. Eng. Jpn 25, 254–264 in Japanese.

Tomiyama, A., Celata, G.P., Hosokawa, S., Yoshida, S., 2002. Terminal velocity of single bubbles in surface tension force dominant regime. Int. J. Multiph. Flow 28, 1497–1519.

Tomiyama, A., Tamai, H., Zun, I., Hosokawa, S., 2002. Transverse migration of single bubbles in simple shear flows. Chem. Eng. Sci. 57, 1849–1858.

Tomiyama, A., 2004. Drag, lift and virtual mass forces acting on a single bubble. In: International Symposium on Two-Phase Flow Modelling and Experimentation.

Vakrushev, I.A, Efremov, G.I., 1970. The velocities of single gas bubbles in liquids. Chem. Technol. Fuels Oils (USSR) 5/6, 376–379.

Wellek, R.M., Agrawal, A.K., Skelland, A.H.P., 1966. Shape of liquid drops moving in liquid media. AIChE J 12, 854–862.